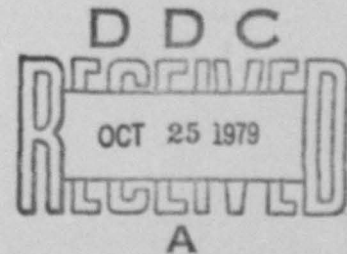# The Nature of Strength Controlling Machining Flaws in Ceramics

R. W. RICE AND J. J. MECHOLSKY, JR.

Ceramics Branch
Material Science and Technology Division

September 25, 1979

NAVAL RESEARCH LABORATORY
Washington, D.C.

79 10 25 152

REPORT DOCUMENTATION PAGE		READ INSTRUCTIONS BEFORE COMPLETING FORM
1. REPORT NUMBER NRL Memorandum Report 4077	2. GOVT ACCESSION NO.	3. RECIPIENT'S CATALOG NUMBER
4. TITLE *(and Subtitle)* THE NATURE OF STRENGTH CONTROLLING MACHINING FLAWS IN CERAMICS		5. TYPE OF REPORT & PERIOD COVERED Interim report on a continuing NRL problem
		6. PERFORMING ORG. REPORT NUMBER
7. AUTHOR(s) R. W. Rice and J. J. Mecholsky, Jr.		8. CONTRACT OR GRANT NUMBER(s) NRL-MR-4077
9. PERFORMING ORGANIZATION NAME AND ADDRESS Naval Research Laboratory Washington, D.C. 20375		10. PROGRAM ELEMENT, PROJECT, TASK AREA & WORK UNIT NUMBERS NRL Problem 63M05-12 and 63P03-19
11. CONTROLLING OFFICE NAME AND ADDRESS		12. REPORT DATE September 25, 1979
		13. NUMBER OF PAGES 32
14. MONITORING AGENCY NAME & ADDRESS*(if different from Controlling Office)*		15. SECURITY CLASS. *(of this report)* UNCLASSIFIED
		15a. DECLASSIFICATION/DOWNGRADING SCHEDULE

16. DISTRIBUTION STATEMENT *(of this Report)*

Approved for public release; distribution unlimited.

17. DISTRIBUTION STATEMENT *(of the abstract entered in Block 20, if different from Report)*

18. SUPPLEMENTARY NOTES

This report serves as a preprint/reprint of the paper by the same title and authors that will appear in the Proceedings of Conference on the Science of Ceramic Machining and Surface Finishing, II.

19. KEY WORDS *(Continue on reverse side if necessary and identify by block number)*

Brittle failure	Fractography	Sanding
Flaws	Grinding	Strength-size effects
Flaw populations	Machining	
Fracture origins	Polishing	

20. ABSTRACT *(Continue on reverse side if necessary and identify by block number)*

The nature of machining flaws introduced in a variety of glass, single crystal, and especially poly-crystal bodies are reported, based on fractographic determination of such flaws as the source of mechanical failure. Particular attention is given to grinding where the anisotropy of strength due to the direction of grinding relative to the tensile axis is shown to be due primarily to a dual population of flaws of differing shapes. One set of flaws form ~ perpendicular and another ~ parallel to the grinding direction. The latter flaws are typically substantially more elongated and often larger than the former and thus give lower

(Continues)

DD FORM 1473 EDITION OF 1 NOV 65 IS OBSOLETE
S/N 0102-014-6601

i

20. Abstract (Continued)

strengths for stressing perpendicular to the direction of grinding. Sawing, sanding, and polishing are also shown to result in similar dual flaw populations. The character of flaws are examined as a function of the type of material and machining, as well as specimen size and shape. The latter suggests a limited strength-size effect due to machining flaws. However, the key findings are that machining flaws do not vary greatly with typical variations of machining or material parameters, e.g. composition, grain size, or hardness.

ii

TABLE OF CONTENTS

THE NATURE OF STRENGTH CONTROLLING
MACHINING FLAWS IN CERAMICS

1. Introduction

Machining of most glasses, single crystals, and dense polycrystalline specimens is typically assumed to introduce flaws which control their mechanical strength. However, in discussing the evidence for such flaw controlled failure versus dislocation controlled failure, Rice [1][2], at the previous Machining Conference, pointed out that there had been little or no direct verification of flaw failure. This paper summarizes and significantly extends recent work on the nature of flaws introduced in a variety of ceramic materials, as a function of various machining and specimen parameters [2-9]. The nature of the two flaw populations that result in the common anisotropy of strength associated with different grinding directions are treated first. Then, more limited studies of other modes of machining are compared with these grinding studies, followed by some discussion of flaw variations and distributions.

---

2. Experimental Procedure

The grinding observations summarized here cover several years involving several machine operators as well as a variety of materials. Grinding was done predominantly, but not exclusively, with 320 grit diamond wheels, most often either with a vitreous bonded wheel (~ 10 cm dia. operating at ~ 7900 rpm) or a metal bonded wheel (~ 20 cm dia. operating at ~ 1725 rpm). A range of feed rates, commonly of the order of 1 cm/sec, and depths of cut, commonly ~ 0.05 mm, per pass and at least two different sizes and styles of grinding machines have been used [3,10,11]. In addition, some observations are from specimens or components of different materials, sizes, and configurations, ground and tested by at least three other organizations. Thus, the results should have broad applicability.

Diamond sawing was with typical diamond saws, e.g. as described elsewhere [10] with cutting rates of the order of 2 cm^2/min for the MgF_2 of this study. Hand sanding was done with 320 or 600 grit SiC paper under dry conditions with finger pressure only. Diamond polishing was typically done to ~ 1 μm grit size on a maple lap with kerosene as a fluid. Some specimens or components were polished and tested in other laboratories.

Mechanical testing was typically by 3 point flexure at ~ 22°C on bars ~ 1.3 x 2.6 mm in cross section on a span of ~ 1.3 cm with a head travel of ~ 1.3 mm/min, but other size and test results are included. Fracture origins were determined on tested samples by optical and scanning electron microscopy using the techniques described by Rice [12].

3. Strength Anisotropy and Flaw Shape as a Function of Grinding Direction

At the previous ceramic machining conference, Rice reported studies showing that an anisotropy of strength resulted in a variety of glasses, single crystal, and polycrystalline flexure bars as a result of stressing relative to the grinding or sanding direction and the bar axis [11]. Characteristically, tensile stresses parallel with the grinding direction, i.e. parallel to the bar axis, gave the highest strength, while tensile stresses perpendicular to the grinding direction gave a lower strength, often by up to 50%. Kirchner also independently reported similar anisotropy of strength relative to the grinding direction of round rods of fine grain Al_2O_3 [13]. Subsequently, other investigators have reported similar anisotropies of strengths especially in hot pressed Si_3N_4 [14] which was also included in Rice's original study.

Rice originally proposed that the cause of this anisotropy of strength was stress concentrations associated with resultant grinding striations or grooves that could be viewed as two facing surface steps, each having a stress concentration associated with it of ~ 1 + 0.7 (h/r) where h is the height of the steps and r is the radius of curvature at the base of the step. Thus, for stressing parallel with the grinding striations there would be no stress concentration while for stressing perpendicular to the direction of grinding the stress being normal to the grinding striations would provide the maximum stress concentrations at the surface steps or grooves. Several subsequent investigators have also generally associated the strength anisotropy with these grinding striations. However, there are two factors which show that these grinding striations are typically not a major factor in the anisotropy of strength associated with stressing relative to the grinding direction.

The first factor showing that the grinding grooves thermselves are probably not the predominant factor in the strength anisotropy as a function of the stress direction relative to the grinding direction is a closer eval-

2

uation of the nature of the grooves themselves and their possible stress concentration. If a grit particle gouged out a simple groove defined by the average upper limit of its protrusion from the grinding wheel, $h \sim r$, it would give an $\sim 70\%$ increase in the component of stress normal to the groove. Thus, if h were of the order of the flaw sizes in ceramics, the $\sim 70\%$ stress concentration would suggest the possibility that the grooves themselves are the source of failure. However, examination of more severe grinding grooves which are typically associated with the flaws causing failure shows that $h/r < 1$, e.g. $\frac{1}{4}$, which is also indicated in the single particle machining experiments of Gielisse et al [15]. This reduces the stress concentration to $\sim 30\%$ or less. While local irregularities in the grooves would locally increase the stress concentrations, these are not likely to extend over a sufficient range to change the situation. Further, the grooves often do no appear to be as deep as typical flaws. Another aspect of the grooves themselves that indicates they are not the predominant cause of strength anisotropy is the fact that they are often not continuous [11], and failure is observed to sometimes occur where grooves have not formed or have been removed by spalling. Note also that correlations between grit particle size and flaw sizes [16-19] do not have to arise from the groove being the flaws. It is quite likely that the different sized grit particles act as different size indentors with larger grit sizes introducing cracks that extend deeper below the surface. Thus, cracks extending in from the surface due to the grooving by the particle may well correlate with particle size. However, because of the increased distance of the crack periphery from the surface steps, the effect of the step stress concentration on the crack would be greatly reduced.

The second, and major factor, showing that the grinding striations themselves are typically not a major factor in the anisotropy of strength as a result of stressing relative to the grinding direction is direct fractographic identification of the nature of flaws from which mechanical failure initiates in specimens. The net result of a substantial amount of study is that there are basically two different sets of flaws extending into the body from the surface generated by grinding (figure 1). Sample fractographs illustrating the difference in shape between the two sets of flaws are shown for fine grain (figure 2), large grain (figure 3), and single crystal bodies (figure 4). Other examples will be shown and discussed later. Additional examples of the two sets of flaws can be seen in references 3-9 and 20-24.

These studies show that one set of flaws form essentially parallel with, and approximately at, the bottom of the grinding groove. The other set of flaws typically form $\sim$ perpendicular to the grinding grooves, apparently due to stick-slip or other dynamic variations in local tensile stresses generated by the machining action $\sim$ parallel with the directions of machining, i.e. of grinding particle motion. Typically, both sets of flaws extend to similar depths. However, the flaws forming along the grinding grooves are characteristically more severe than those forming perpendicular to the grinding grooves consistent with the observed strength anisotropy. The greater severity of the flaws along the grinding grooves is generally due more to their greater length rather than their depth (figures 1-4).

Analysis of extensive observations of the anisotropy in flaw shape between the two sets of flaws on strength is given in table 1. Here the observed anisotropy of strength is compared with the strength anisotropy predicted from the Griffith equation using the observed flaw size and shape parameters. This clearly shows that the anisotropy in flaw shape is typically the overwhelming factor in the strength anisotropy.

In addition to the above more detailed, quantitative studies, a variety of qualitative observations further extend the scope of the observation of strength anisotropy being due to the differences in shape of the two flaw populations associated with machining as indicated in table 2. Thus, for example, in studies of hot pressed Si_3N_4, limited determinations of machining flaws at fracture origins of bars machined parallel with the tensile (bar)

3

TRANSVERSE
CRACKS

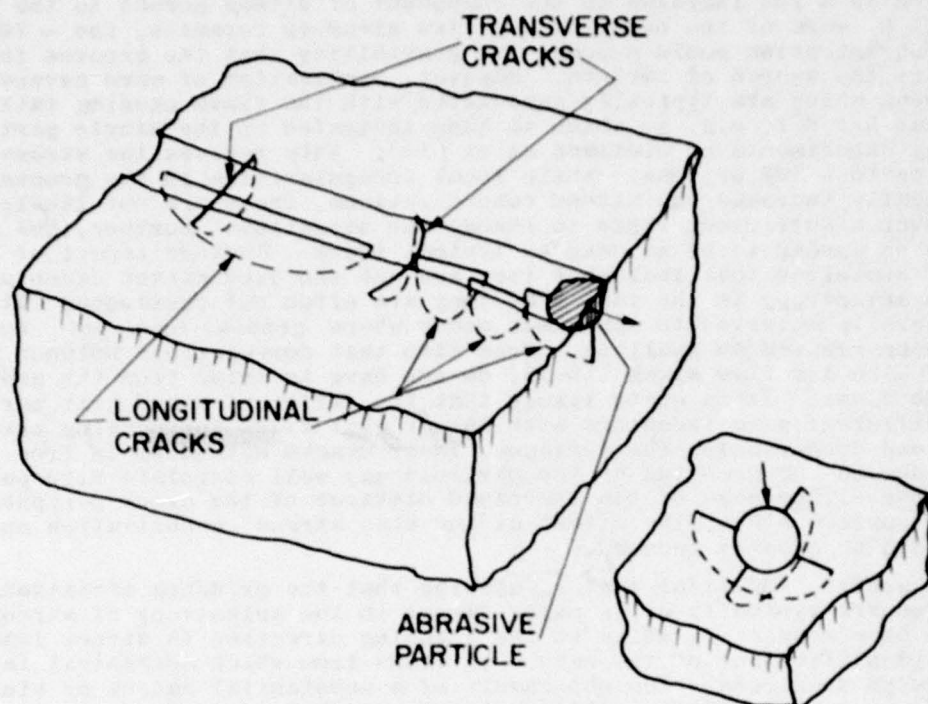LONGITUDINAL
CRACKS

ABRASIVE
PARTICLE

Figure 1. Schematic representation of flaws introduced in scratching a
  ceramic surface. While the main focus of the schematic is the effect of
  an abrasive grit particle on the surface of the ceramic, it is also rea-
  sonably representative of what commonly happens in a scratch hardness
  type test. One of the main differences between these two types of scratch-
  ing operations is that in the abrasive machining operation extensive spal-
  ling often occurs along the path of the grit particle which is not shown
  in order to keep the schematic simple. Such spalling may or may not occur
  in the scratch hardness type test depending for example on the load and
  material.   This sketch schematically summarizes the basic findings of ex-
  tensive observations on machining flaws which are also generally consistent
  with observations made from scratch testing; namely that the motion of
  particle or an indentor over the surface introduces two sets of flaws ex-
  tending into the body from the surface. One set of flaws is essentially
  parallel with the groove. Such flaws are typically reasonably elongated
  either in a fairly continuous fashion or in a more irregular fashion due
  to the partial or complete overlap of a number of shorter flaws. The
  second set of flaws are typically approximately perpendicular to the mo-
  tion of the particle or point and their periphery often approaches a semi-
  circle. While some of the second type of flaws may be relatively planar
  they often have some concavity towards the direction from which the par-
  ticle or point approached the point where the flaw initiates. The insert
  to the right schematically illustrates the approximate analogue for a
  static indentation. While for simplicity, a round particle has been shown
  from which more than two sets of flaws might well form in a simple indenta-
  tion test only two have been shown here since this would tend to be more
  representative of the angular nature of particles similar to what one ob-
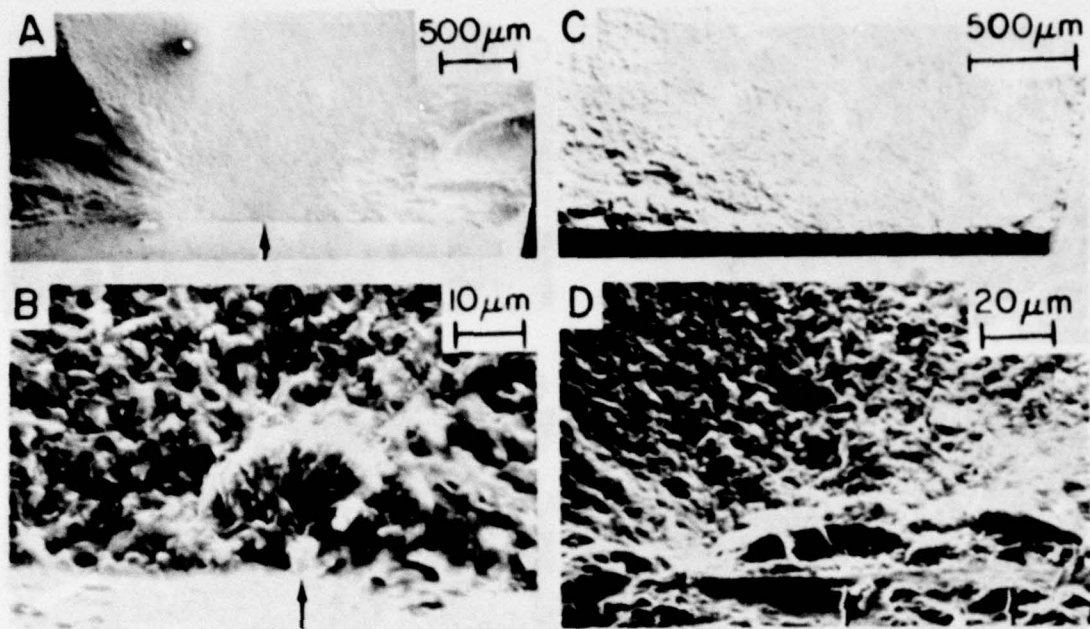 tains with an angular, e.g. Vickers, indentor.

4

Figure 2. Example of machining flaws at fracture origins in a fine grain ceramic machined parallel and perpendicular to the tensile axis of the bar. A and B represent lower and higher magnification of the fracture origin of a dense, fine grain mullite bar machined parallel with the tensile axis; fracture stress ~ 325 MPa (47,000 psi). Note the nearly semicircular, i.e. half-penny shape of the flaw periphery, but that the flaw has some curvature to it, e.g. its shape is similar to half a clam shell. Figure C and D show fracture surfaces and the fracture origin of a test bar of the same material ground perpendicular to the tensile axis; fracture stress ~ 207 MPa (30,000 psi). Note some difference in depth of the flaws in A-D, the more elongated character of that in C and D, and the fact that the latter consists of at least two partially over-lapping segments.
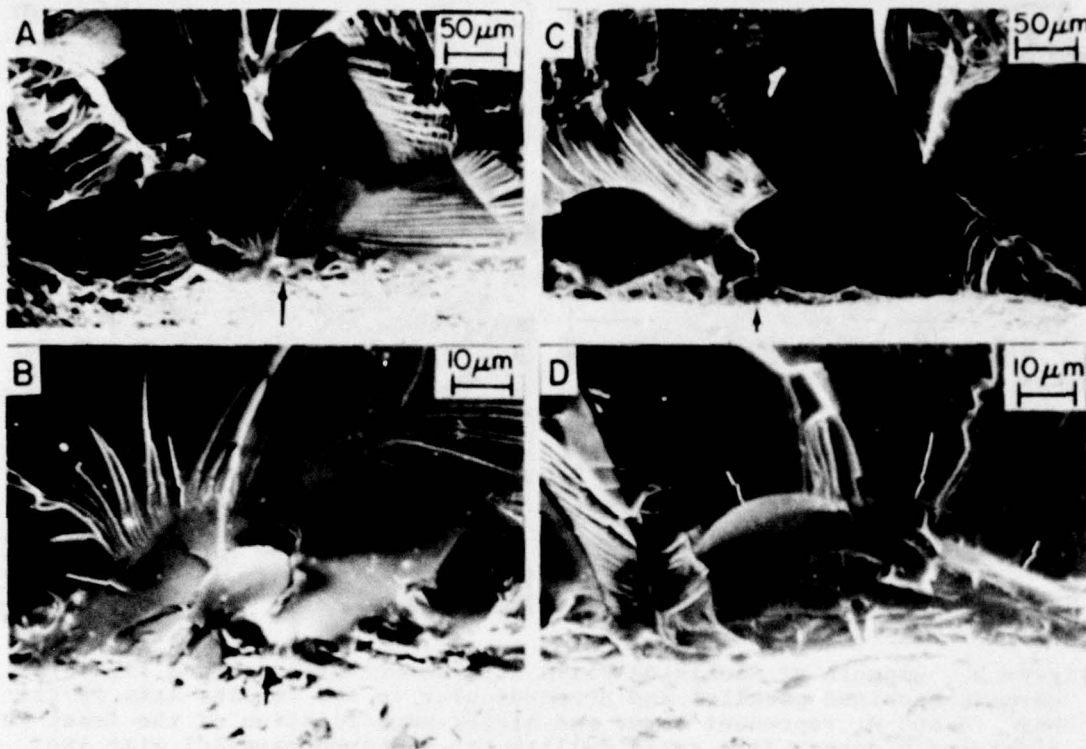
Figure 3. Examples of machining flaws at the fracture origins for parallel
and perpendicular machining of a large grain ceramic. A and B show
the fracture origin area and the specific failure causing flaw (arrows)
as a result of grinding a dense, sintered Y_2O_3 (Yttralox) bar parallel
with the tensile axis. Note the nearly semicircular nature of the final
flaw boundary and that the flaw is substantially less than the size of
the grain in which it formed. C and D show the fracture surface and
fracture origin (arrows) of a specimen of the same material ground per-
pendicular to the tensile axis. Note the more elongated character of
the flaw but that it is again substantially smaller than the size of
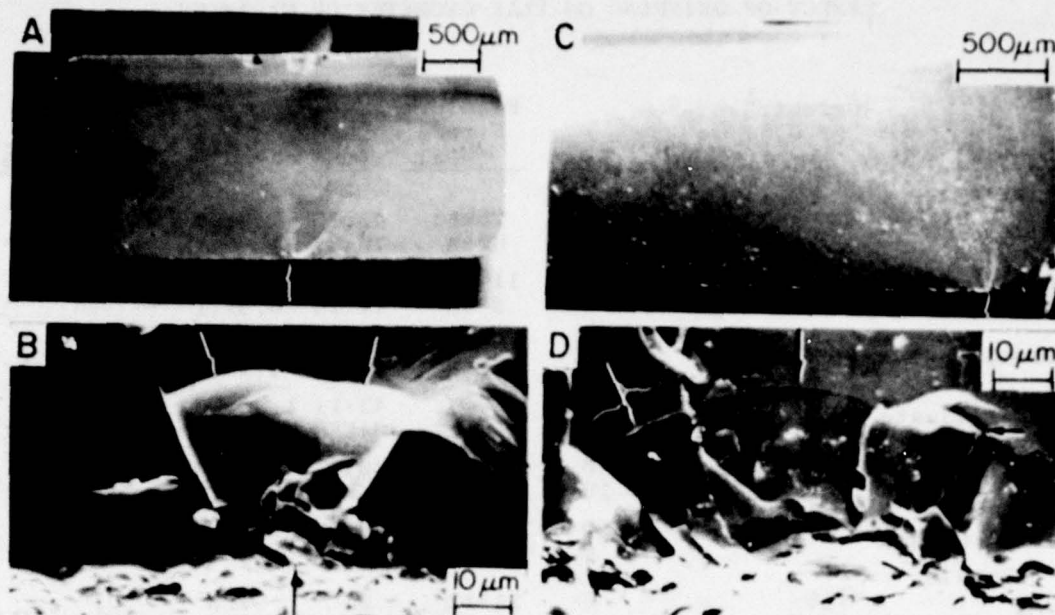the grain in which it is located.

6

Figure 4. Examples of flaws at the fracture origins in parallel and perpendicular ground $MgAl_2O_4$ single crystal. A and B show the fracture surface and fracture origin (arrows) of a stoichiometric $MgAl_2O_4$ crystal ground parallel with the <100> tensile axis and having a [110] tensile surface, fracture stress ~ 145 MPa (21,000 psi). C and D show the fracture surface and origin (arrows) of a sample of the same material and orientation ground perpendicular to the tensile axis; fracture stress ~ 117 MPa (17,000 psi). While the flaw shapes shown here are somewhat more irregular than often observed, the flaw causing failure from machining parallel with the tensile axis is definitely of similar depth but less elongated than that causing failure from machining perpendicular to the tensile axis.

axis show the flaws to commonly approach ~ half penny flaws, while more extensive observations on specimens ground perpendicular to the tensile axis both in the form of flat bars and round tensile specimens clearly show much more elongated flaws [20, 21] (see also fig. 18). Similarly, large round tensile specimens of Al_2O_3 which were ground circumferentially [22], i.e. perpendicular to the tensile axis characteristically show more elongated flaws at fracture origins than observed in Al_2O_3 or other materials ground parallel with their tensile axis. Also, limited studies of β-Al_2O_3 bars ground perpendicular to the tensile (bar) axis show more elongated flaws at fracture origins than the ~ penny shaped machining flaws at fracture origins of bars ground parallel with the tensile axis [23]. There are also preliminary indications of strength anisotropy in a cermet (table 2). Finally, Richerson has shown evidence of grinding direction dependent strengths in some denser reaction sintered Si_3N_4 [24] consistent with other observations of machining flaws in such material [20,21].

The observations of this section on two sets of flaws from grinding, one set forming generally parallel with and essentially ~ along the bottom of the grooves generated by the individual grinding particles and the other

7

TABLE 1

EFFECT OF GRINDING ON FLAW GEOMETRY OF CERAMICS

Material	Orient.[1] or G.S. (μm)	G.D.[2]	No.[3]	Fracture Stress (MPa)	c[4] (μm)	a/b[4,5]	$\sigma_\perp/\sigma_\parallel$[6]	B[7]
A. Glasses:								
Silica		‖	7	73±10	45±16	1.3±.4	0.84	0.86
		⊥	4	62±8	75±37	1.0±.4		
Alumino-silicate		‖	12	117±10	39±9	1.6±.2	0.68	0.69
		⊥	5	80±7	71±10	0.5±.1		
Borosilicate		‖	3	99±8	35±6	0.9±.3	0.9	0.9
		⊥	4	92±9	39±9	1.1±.3		
Lead Silicate		‖	7	69±3	43±17	1.35±.6	0.86	0.82
		⊥	7	59±17	64±38	1.26±.8		
Soda Lime		‖	25	97±5	28±9	1.6±.2	0.65	0.65
		⊥	16	68±8	67±5	0.5±.2		
Glassy Carbon		‖	10	94±9	40±9	0.9±.3	0.93	1.03
		⊥	9	87±18	35±15	1.2±.6		
B. Crystals:								
TiO$_2$	$\langle\bar{1}10\rangle$	‖	6	113±7	25	0.7	1.1	0.9
	(110)	⊥	6	120±4	30	0.7		
TiO$_2$	$\langle1\bar{1}0\rangle$	‖	5	113±3	30	1.5	0.7	0.7
	(001)	⊥	5	77±3	70	1.5		
TiO$_2$	$\langle010\rangle$	‖	6	288±19	--	--	0.83	--
	(100)	⊥	5	239±12	25	1.3		
TiO$_2$	$\langle010\rangle$	‖	5	108±6	60	1.3	1.0	0.9
	(001)	⊥	5	103±6	70	1.3		
TiO$_2$	$\langle001\rangle$	‖	8	285±86	10	0.4	0.6	0.5
	(100)	⊥	7	183±36	35	0.18		
MgAl$_2$O$_4$	$\langle100\rangle$	‖	3	217±28	15±0	0.4±0.6	0.8	0.8
	(110)	⊥	3	165±28	14±7	0.4±0.6		
C. Polycrystals:								
Keatite Glass Ceramic	< 1	‖	6	180±39	16±5	0.9±0.4	0.6	0.5
		⊥	7	102±8	36±15	0.5±0.2		
MgF$_2$	< 1	‖	10	87±2	54±21	1.1±.07	0.6	0.6
		⊥	10	53±2	89±20	0.5±.08		
Mullite	1-3	‖	7	319±35	41±23	1.0±0	0.8	1.0
		⊥	6	259±54	24±5	0.4±0.3		
B$_4$C	2-10	‖	5	374±69	19±3	1.0±0	0.6	0.8
		⊥	9	154±24	26±10	0.2±0.07		
B$_4$C	100-200	‖	4	282±228	19±9	0.7±0.5	0.9	0.7
		⊥	6	250±55	23±3	0.3±0.2		
CaF$_2$	50-150	‖	3	50±13	23±7	0.7±0.2	0.8	0.8
		⊥	3	40±5	33±7	0.6±0.6		
Yttralox	100-200	‖	6	99±6	36±13	0.8±0.3	0.8	0.9
		⊥	7	77±8	44±20	0.7±0.3		

---

[1] Orientation of single crystals < > gives tensile axis, and ( ) tensile sur-

8

face. G.S. = grain size.

[2]G.D. = grinding direction relative to tensile axis.

[3]No. = number of specimens.

[4]c = smallest flaw dimension (smallest of a or b below).

[5]b = flaw half length along surface; a = flaw depth.

[6]Ratio of fracture stress for perpendicular to parallel grinding.

[7]$B = \dfrac{\Phi_\perp}{\Phi_\parallel} \sqrt{\dfrac{c_\parallel}{c_\perp}}$ where $c_\parallel$ and $c_\perp$ are the smallest flaw dimension for parallel and perpendicular grinding respectively and $\Phi_\parallel$ and $\Phi_\perp$ are respective elliptic integrals for the flaw shapes.

TABLE 2

OTHER MATERIALS IN WHICH GRINDING DIRECTION EFFECT HAS BEEN INDICATED[1] BY

Material[2]	σ[3]	a,b[4]	Material[2]	σ[3]	a,b[4]
Sapphire	x	x	ZrO$_2$-fine grain partially stabilized	x	x
H.P. Al$_2$O$_3$	x	x			
S. Al$_2$O$_3$	x		H.P. SiC	x	x
H.P. Mullite	x	x	H.P. Si$_3$N$_4$	x	x
H.P. β-Al$_2$O$_3$	x	x	75% TaC-25 Inconel[5] Cermet	x	

---

[1]In studies by the authors.

[2]S = sintered, H.P. = hot pressed.

[3]σ = strength, i.e. strength anisotropy.

[4]a,b = flaw depth and half length, i.e. flaw geometry.

[5]From selection of bars with ~ circular pattern milling or grinding marks ~ ∥ to tensile axis (173 ± 33 ksi) and ~ ⊥ to tensile axis (140 ± 38 ksi) for 3 spec. each.

set generally forming ~ perpendicular to those grooves, are consistent with cracking patterns observed over a period of years by a variety of investigators for both static hardness impressions and especially dynamic, i.e. scratch, hardness grooves [25-29] including earlier work, Brüche and Poppa [25, 26].   Note also that the flaws ~ perpendicular to the grinding direction have a curvature consistent with that expected for the motion of the grinding particles. Thus, while there are variations in these two sets of flaws, they are a basic aspect of grinding as well as other machining processes as will be discussed later.

Before proceeding with a more detailed description of machining flaws and variables effecting them, it is appropriate to briefly consider the detection of these flaws and their meaning. Typically, the flaws observed are believed to be the original machining flaws for two reasons. The first

of these is based on the fact that cracks typically propagate normal to the tensile stress causing their propagation. Thus, since the orientation of the stress forming the crack during machining can almost never be duplicated by the applied stress causing failure, the crack will be propagated on a somewhat different surface than that on which it originally formed. This change of surface results in a demarcation, which is generally detectable unless failure is nearly or completely intergranular, in which case the demarcation is generally obscured by the grain to grain variation of the crack topography. Since other possible changes in local stress around a crack due to crack velocity effects are much more subtle, if they exist at all, the demarcation between the original flaws and its first subsequent motion for failure are clearly predominant and typically what is observed. This is a major reason why the purely qualitative speculation of Doremus [30] that similar flaws they observed at the fracture origins of machined glass bars represent not the original flaws but some intermediate stage of failure should be rejected.

The second reason that the demarcations seen are attributed to the original flaws rather than some stage of subsequent propagation is due to changes in fracture mode that can occur during some stage of propagation. Mecholsky et al have shown that environmentally induced slow crack growth often proceeds intergranularly in polycrystals, e.g. MgF_2 [31]. Thus, since both the original machining flaws and the subsequent final fast fracture are mainly, or exclusively, transgranular in nature, the slow crack growth region is clearly defined showing the flaws such as those in this paper to typically be the original flaw and not involving some subsequent subcritical growth.

4.   Other Aspects of Machining Induced Flaws

4.1   Microstructure, Composition and
Machining Flaws from Grinding

Extensive studies of interaction of machining flaws with porosity have not been conducted. However, a number of observations indicate that isolated pores near the surface can be connected to the surface by machining flaws, e.g. figure 5. See also figure 13C and D.

Substantially, more extensive observations have been made on the effect of grain size on machining flaws. The essential result is that over the typical range of grain sizes encountered there is at best a limited decrease in the depth of flaws introduced by machining with decreasing grain size. Thus, for example, note the similarity in flaw sizes of specimens of comparable size for single crystals and polycrystals of $MgAl_2O_4$ of different grain sizes (compare table 1 and figure 4 with figure 3 of reference 22), different grain sizes of B_4C (table 1) and single and polycrystalline flaws in Al_2O_3 [22]. A variety of other more limited, e.g. non-quantitative observations, support this. For example, note the machining flaw at a possible, but uncertain, fracture origin in large grain CVD in figure 6 has ~ the same depth as the typical flaws observed in fine grain hot pressed Si_3N_4 (see references 20 and 21 as well as figure 18).

Further, note in general that there are limited differences in flaw depths and no systemmatic pattern between materials of different compositions and hence of differing properties such as hardness. Thus, note the typical flaw sizes for the variety of materials of similar specimen size and a common machining direction, do not vary over a significant range (table 1). This further reinforces the limited effect of grain size on the size of machining flaws that control strenght (e.g. compare figures 2-4). The ramifications of the observation that there is little or no dependence of the size of machining flaws on grain size of the body being machined, are discussed in another paper [22].

10
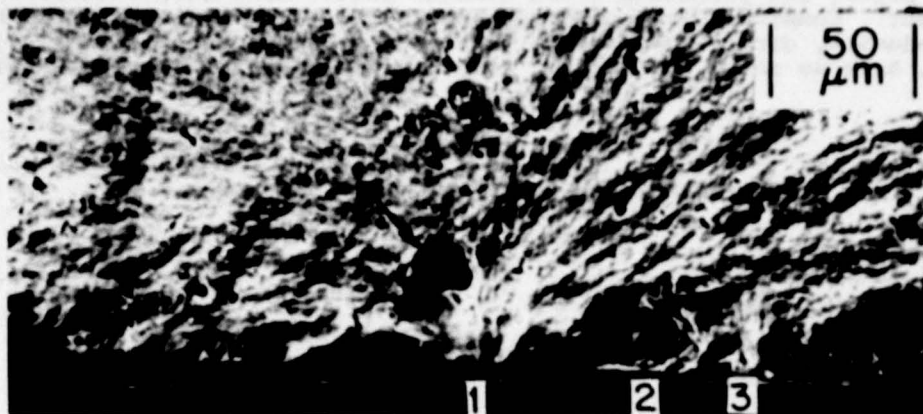
PZT $\sigma_f \sim 15$ KSI

Figure 5. Example of pore-machining flaw interaction as a source of failure. On the fracture surface of this commercial lead zirconate titanate sample, three similar size machining flaws can be seen along the surface. Flaw 1 has connected with a pore, P, somewhat below the surface, to form the primary source of failure. Flaws 2 and 3 indicate two other machining flaws.
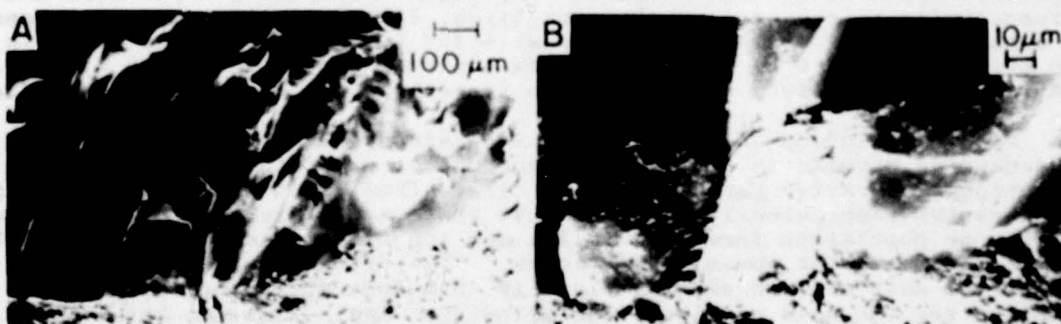

Figure 6. Grinding flaw in large grained Si_3N_4. A and B show respectively lower and higher magnification of a probable fracture origin and probable flaw (arrows) causing failure in this large, columnar grain, CVD Si_3N_4. Note also the two or three nearly concentric markings suggesting progressive stages of flaw development. Such markings with varying spacings are observed fairly frequently with flaws forming approximately perpendicular to the direction of machining. Photo courtesy of Dr. Carl Cm. Wu.

11

4.2. Machining Flaws from Other Modes of Abrasive Machining

Three other major modes of machining, diamond sawing, hand sanding with abrasive paper, and polishing (with diamond paste) have been studied to varying extent. Consider first diamond sawing. While extensive studies have not been conducted, direct comparisons have been made using optical grade, hot pressed, MgF2 as shown in table 3. The circular nature of the blade leaves

TABLE 3

FLEXURAL STRENGTH OF AS-DIAMOND SAWN MgF_2*

Bars	No. of Tests	Strength MPa	ksi
0.36 x 0.65 cm 1.9 cm span	10	71 ± 21	10 ± 3
0.23 x 0.55 cm 1.27 cm spann	3	100 ± 23	15 ± 3

*Kodak IR window grade tested in 3 point flexure with a 1.27 mm/min head travel rate.

an arc of "sawing" grooves with, in turn, presumably result in a directionality of the strength of diamond sawn specimens if they were tested as a function of such orientation. This has not been explored, most specimens had the sawing grooves at intermediate angles (e.g. ~ 45°) to the tensile axis. The strengths of typical laboratory size bars as a result of such diamond sawing are in the same range but somewhat less than those from diamond grinding. Fractographic studies in this material, which is excellent for such studies, show definitive flaws at fracture origins from diamond sawing. These flaws are very clearly associated with more extreme surface grooves. Again both sets of flaws, i.e. those essentially ~ parallel and ~ perpendicular to the grooves are seen (figs. 7 and 8) with the former tending to dominate failure with the grooves at ~ 45° to the tensile axis.* Both the strengths (table 3) and actual flaw observations (figs. 7 and 8) show similar size flaws from sawing as from the comparable direction of grinding.

Previous studies have shown that stressing relative to the direction of hand sanding results in a similar anisotropy of strength relative to the direction of abrasive particle motion [11]. Thus, hand sanding (dry) with SiC abrasive paper clearly suggests that there are again two populations of flaws, one population forming parallel and the other forming perpendicular to the motion of the abrasive particles. The difference in the shapes of the two sets of such sanding flaws is thus apparently very similar to those of the two sets of flaws from grinding. Again limited, but definitive, observation support this conclusion, e.g. note the character of flaws associated with hand sanding (fig. 9) of very fine grain, high strength SiC resulting from the CNTD† process [32]. It should be noted that this similarity suggests that the differences between grinding and sanding, e.g. orders of magnitude difference in abrasive particle velocity have a limited effect

*Such results indicate that much study of mixed mode failure can be done directly with machining flaws by varying the angle of machining relative to the tensile axis, rather than using artificial indent induced flaws.
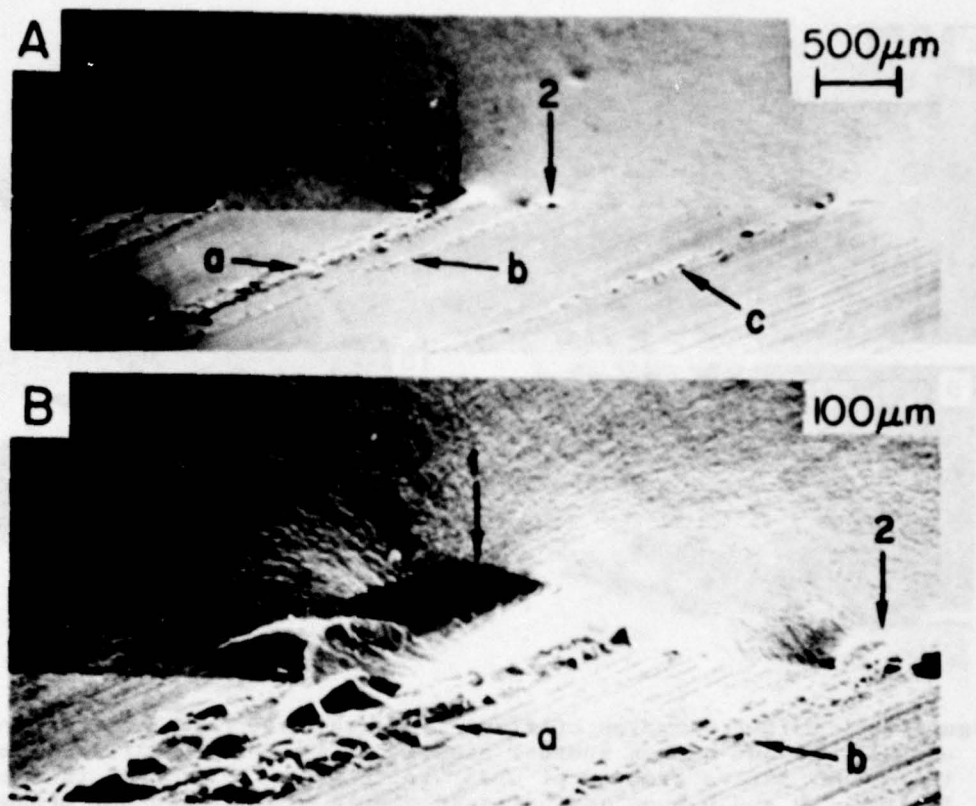
†Essentially a modified chemical vapor deposition process.

12

Figure 7. Examples of machining flaws in MgF_2 from diamond sawing. A and B show the fracture surface in the vicinity of the fracture origin (upper part of photos) and part of the machined tensile surface (lower portion of photos) of dense hot pressed optical grade MgF_2. Note the deeper sawing grooves at ~ 45° to the tensile axis and that each of these appears to have a machining flaw associated with it on the fracture surface e.g. note flaws 1 and 2 associated respectively with sawing scratches a and b in both photos. The larger flaw, 1, is clearly the origin of failure. Note that this flaw is somewhat less elongated than average for being ~ parallel with the machining groove. Fracture stress ~ 59 MPa (8,600 psi)
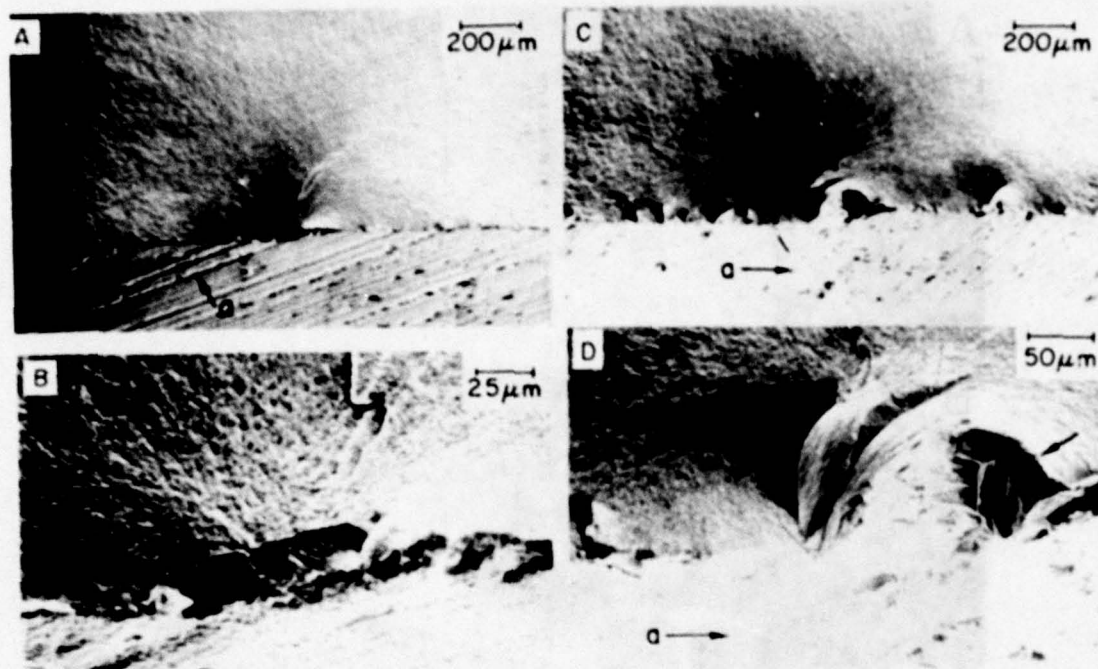
Figure 8. Further examples of flaws from diamond sawing at fracture origins of MgF_2. A and B show another example of an elongated flaw along one of the deeper sawing grooves at ~ 45° to the tensile axis as the source of failure. C and D show another sawn sample of the same hot pressed optical grade MgF_2 failing from sawing flaws where the sawing grooves are ~ parallel with the tensile axis. This illustrates the more complex character of flaws that sometimes can be encountered. Failure appears to have occurred from two flaws; i.e. from part of a flaw parallel to the grinding groove (1 in D) and part, or all, of a flaw ~ perpendicular to the grinding groove. The apparent intersection of two such flaws at the fracture origins is rare but illustrates some of the complications that can arise.
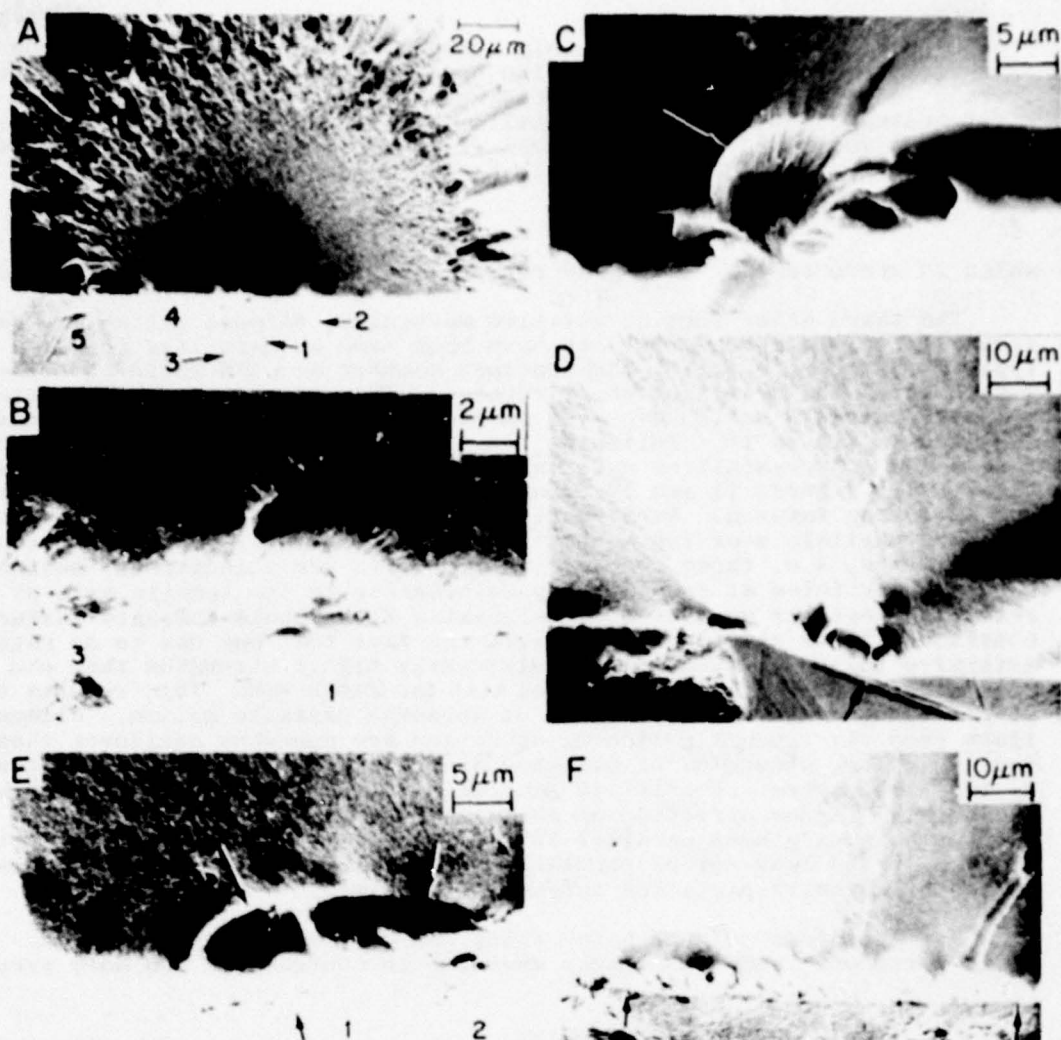
14

Figure 9. Examples of flaws from sanding CNTD SiC. A and B represent lower and higher magnifications of the fracture origin in a sample sanded ~ parallel with the tensile axis. Note the nearly semi-circular nature of the periphery of the flaw causing failure and its curved character. Note also that it is associated with a somewhat discontinuous sanding groove,(1). Note also that each of the other sanding grooves marked 1 through 5 in A has a flaw associated with them, but smaller than the flaw, F, which caused failure. Note also that some of the other flaws are parallel with the grinding groove, e.g. the flaw associated with scratch 3, and hence results in a short vertical step on the fracture surface. A number of cases of this type of behavior are observed for machining falws, further reinforcing the concept of the two flaw population observed here. C, D, E, and F are photos of flaws at the origin of different specimens. Note the generally progressively more elongated character of the flaw or portion of the flaw exposed on the fracture surface as the angle of the scratch forming the flaw increases relative to the tensile axis. The much smaller flaw sizes in this material may reflect in part its extremely fine grain size, e.g. 0.2 μm, but may also be significantly affected by the apparently fairly high residual stress that may exist in these bodies. They, however, provide an excellent opportunity for observing such scratches

15

and the resultant flaws not only because the fine grain size allows more definitive fractography, but also because they have a near pristine surface to begin with, i.e. producing strengths of the order of up to or exceeding 3,500 MPa (500,000 psi). The failure stress of the specimens were as follows: A, B - 1170 MPa (170,000 psi); C - 986 MPa (143,000 psi); D - 778 MPa (113,000 psi); E - 606 MPa (88,000 psi); F - 220 MPa (32,000 psi).

which is predominately of degree rather than of a kind on the flaws generated.

The third other form of abrasive machining, diamond polishing, has been investigated some. Observations have been made on materials polished in a typical fashion, i.e. with the specimen mounted on a disk which is allowed to rotate while the polishing wheel rotates. This results in a net pattern of abrasive particle motion over the surfaces which is essentially random as sketched in figure 10. Polishing flaws observed at fracture origins of single and polycrystalline materials studied to date are highly elongated flaws, e.g. figures 11 and 12, consistent with all of the above results in the following fashion. As a result of the essentially random motion of the abrasive particle over the surface, one should always have some of the most severe flaws, i.e. those forming parallel with the direction of motion of abrasive particles at or near perpendicularity to the tensile axis of the resultant test bar so that these elongated flaws would dominate failure as observed. It is also consistent with the fact that one has to do rather extensive polishing to obtain significantly higher strengths than can be obtained by diamond grinding parallel with the tensile axis. This results because of differences in the consistency of abrasive particle motion. Although the flaws from the typical polishing operation are somewhat shallower than those from grinding, strengths of polished specimens are typically being controlled by the more severe set of flaws generated by abrasive motion because of the essentially random direction of abrasive across the specimen. On the other hand, specimens ground parallel to the tensile axis have their strength controlled by the less severe population of flaws generated by the consistent motion of abrasive particles across the specimen.

Two factors should be noted about the polishing flaws observed. First, their periphery tends to be much smoother in contrast to the more irregular
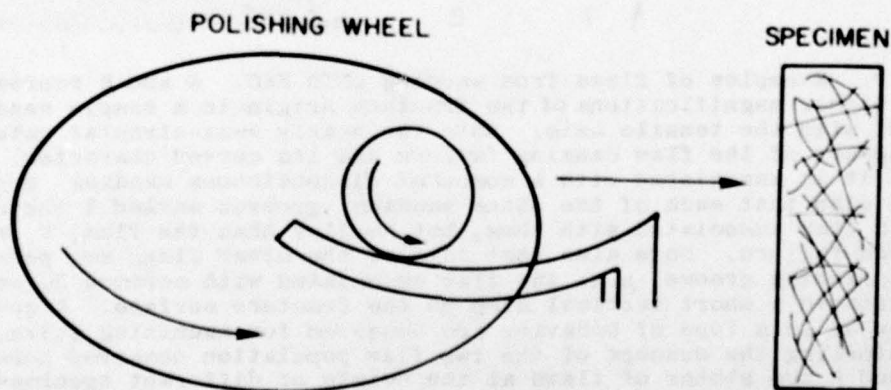

Figure 10. Schematic representation of the common polishing operation and resultant particle and scratch patterns on the surface of the specimen. Typically, these will approach a random pattern; hence the most severe flaws, i.e. those formed essentially parallel with the particles will dominate failure, even in uniaxial stressing.
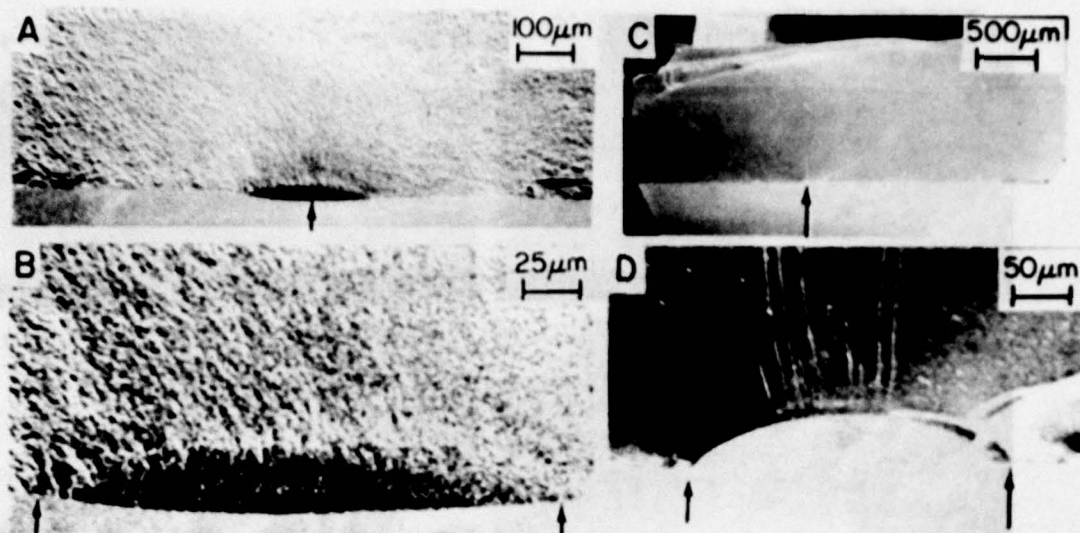
16

Figure 11. Examples of ceramic polishing flaws. A and B show the area of fracture and the fracture origin (arrows) of a fine grain polycrystalline body (hot pressed, optical grade MgF$_2$) as a result of polishing. This sample was tested in biaxial flexure, failure stress ~ 91.6 MPa (13,300 psi). Note the elongated character of the flaws as well as their relatively smooth periphere, in contrast to the commonly much more irregular shape of such elongated flaws from grinding. See figure 17 for another similar example. C and D show the fracture origin area and fracture origin (arrows) of a polished specimen of Al$_2$O$_3$-rich MgAl$_2$O$_4$ (Verneuil) single crystal.

nature of elongated flaws from grinding. As shown in Sections 3 and 4.3, the elongated flaws from grinding are often more irregular, e.g. due to their being made up of a series of smaller flaws of varying degrees of overlapping character. This smoother character of polishing flaws may well represent either, or both of, two aspects of the polishing operations relative to the grinding operation. The much slower motion of the abrasive particles may directly be the cause of the much smoother nature of the flaw periphery due for example to less variation in friction. On the other hand, the slower speed of the abrasive particles may indirectly be effectively allowing more opportunity for stress corrosion or other phenomena to result in a smoother crack periphery during machining flaw formation. Secondly, it should be noted that while there are some differences between grinding and polishing flaws, overall the general nature of the flaws introduced appears to be similar. This again suggests that the velocity and forces associated with different abrasive processes are not a major factor in a character of the flaws that are introduced, but only result in varying degrees of the flaw parameters, e.g. their depth and smoothness.

4.3.   Machining Flaw Distributions and Strength-Size Effects

An important set of questions is: 1) how variable are the flaws from machining in terms of size, shape, and orientation; and 2) how do such variations compare with the observed dependence of strength of specimens on their size and shape due to the differences in the amount of surface or volume under significant stress. While much yet needs to be done in terms of detailed studies of the variation and statistical distribution of the different
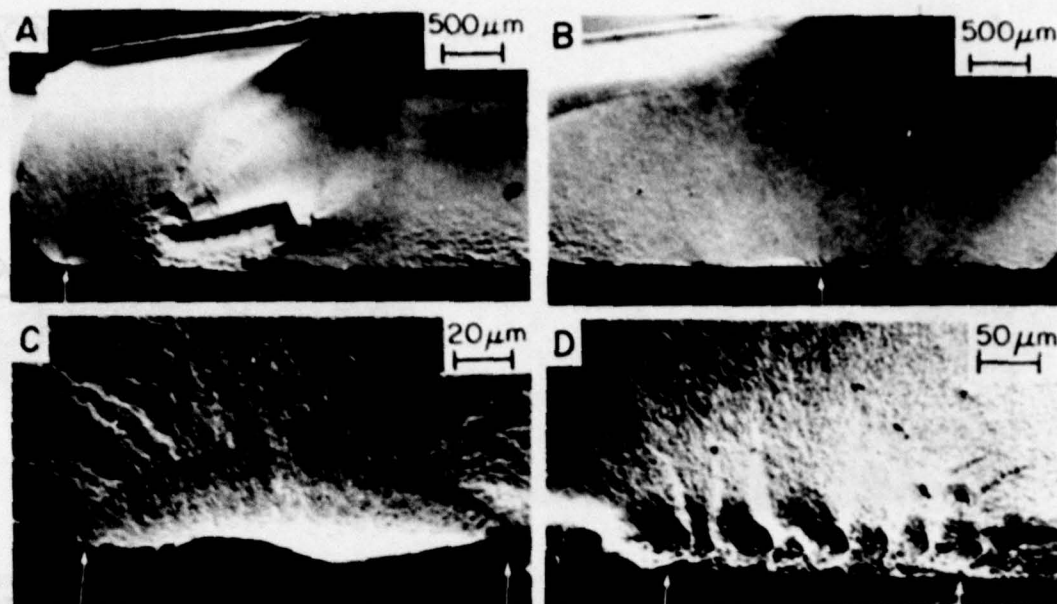
17

Figure 12. Examples of variation of grinding flaws in hot pressed, optical grade MgF$_2$. A and B are fracture photos of the area of origin and the failure causing flaw (arrows) from grinding parallel with the tensile axis, fracture stress ~ 64 MPa (9,300 psi). Note the unusually elongated character for a flaw forming perpendicular to the direction of grinding. This may be in part due to the fact that this flaw is next to the edge of the sample. C and D show the fracture origin and failure causing flaw (arrows) in a sample of the same material ground perpendicular to the tensile axis; failure stress ~ 50 MPa (7,200 psi). This shows a somewhat more exaggerated, but not extreme, example of the type of variation that one can have in flaws forming essentially parallel with the grinding groove.

types of machining flaws, some important observations can be made at this time.

A variety of statistical variations of flaws are observed. One of the most frequent and obviously expected variations of flaws forming parallel and ~ along the bottom of the grinding grooves is their extent and regularity. Basically, these often appear to be not one flaw, but a series of flaws that partially or totally overlap, e.g. see figures 2,3,4,8,9, and 12. For flaws of the type characteristically perpendicular to the grinding grooves, a limited but definite number are observed forming at a variety of angles to the grooves, e.g. figure 13. In finer grain bodies, these angular variations represent sporatic variations of the material or variations of the local machining conditions. However, in larger grain bodies, and single crystals, especially non-cubic ones where planes of the same cleavage system may not be orthogonal, orientation of preferred fracture planes can also be important, figure 13C, D.

Also, some flaws of the type typically forming perpendicular to the grinding grooves may also be wider, i.e. more eccentric than ~ half penny flaws. Again local variations in grinding forces, e.g. a deeper grinding groove or flaw forming between grinding grooves (e.g. see reference 20, 21), as well as local variations in material properties. Another variation, especially with flaws of the type forming perpendicular to the grinding grooves are two to several ~ concentric markings before the final flaw boundaries,
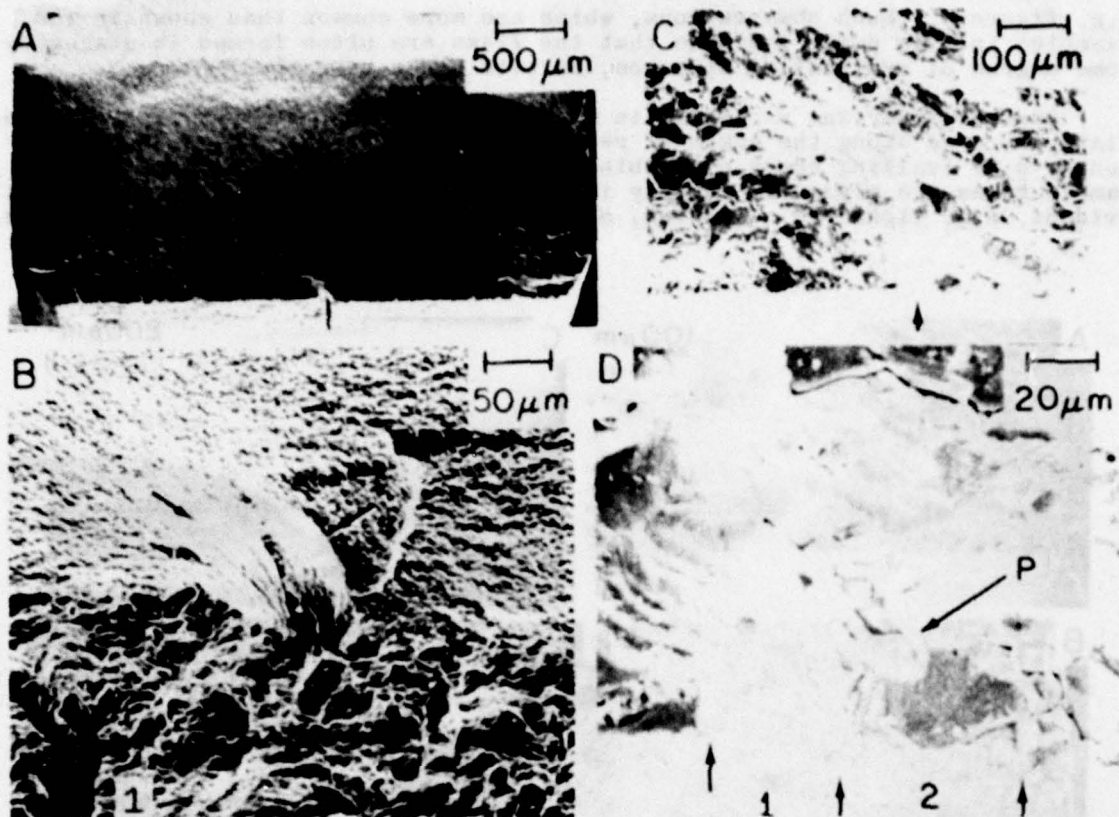
18

Figure 13. Examples of variation in flaws forming approximately perpendicu-
lar to the direction of grinding. A and B are fracture photos of the area
of origin and the fracture origin arrows in a specimen of fine grain,
dense mullite, fracture stress ~ 206 MPa (30,000 psi). Note that the flaw
is at a substantial angle and has substantial curvature relative to the
fracture plane and the tensile axis. While some such flaws may actually
be the continuation, or a curved end, of a flaw forming parallel with the
grinding direction, clearly many of them are not and are simply variations
of the angle of flaws forming perpendicular to the direction of grinding.
This sample represents an extreme misorientation of such flaws. Note also
that there is no obvious deep grinding groove associated with this flaw
and that there is a definitive grinding groove to the left of it in B.
C and D are photos of the area of fracture origin in dense, hot pressed
SiC, failure stress ~ 372 MPa (54,000 psi). While the specific fracture
origin and the machining flaws are both less well-defined, 1 is a fairly
probable machining flaw and 2 is a possible machining flaw in D. Note
that these are ~ equal to the grain size and that neither is associated
with obvious grinding grooves. Note also the substantial angle of 1
relative to the direction of grinding and the tensile axis may be as
much or more due to the orientation of the grain in which it formed,
e.g. due to the orientation of a preferred cleavage plane in that grain,
rather than a statistical variation in the machining or material parame-
ters governing the formation of cracks.

19

e.g. figure 6. Such observations, which are more common than shown in the examples in this paper indicate that the flaws are often formed in stages by some degree of oscillating stresses, or with other vibration.

Another important variation in machining flaws is the formation of edge flaws, such as along the edges of rectangular test bars or edges of components, e.g. trailing edges of turbine blades. While fracture origins from sample edges are generally readily identified, specific flaws are not always evident, e.g. figure 14. However, a substantial number have been identified,
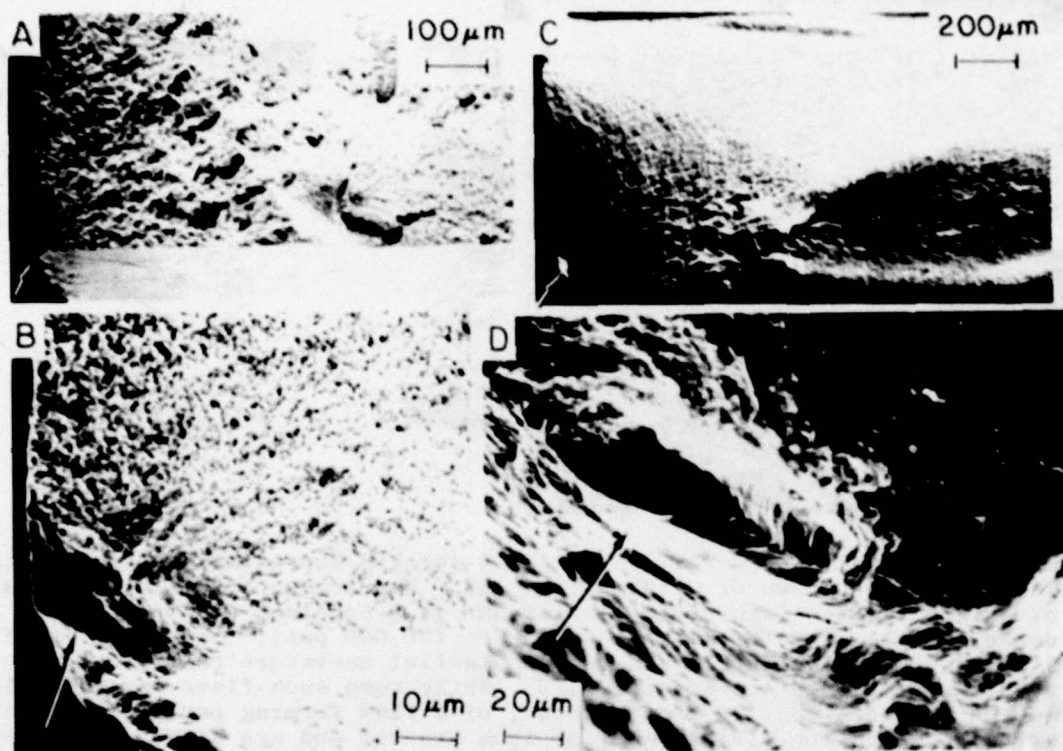

Figure 14. Examples of ill-defined edge flaws at fracture origins in fine grained ceramics. A and B are fracture photos showing the origin of a fine grain ZrO_2 body partially stabilized with 8 w/o Y_2O_3, fracture stresses 276 MPa (40,000 psi). C and D are similar photos of fine grain, dense mullite, failure stress ~ 296 MPa (43,000 psi). Note that the specimens failed from one of their edges are quite definite and usually fairly readily determined but the specific flaw size and shape often cannot be defined, though first approximation would simply be to use the approximate dimensions of the edge chip in A and B, or lip in C and D as a flaw dimension. Such fracture origins are quite common for specimens failing from edges.

20

some of which may be close to a quarter ellipse or circle, but there can be a variety of shapes as indicated in figure 15. An example of an edge flaw in hot pressed Si_3N_4 is shown in reference 21. Some indications of the frequency with which such flaws can occur are given elsewhere [4]. It has also been shown that while such edge flaws may be more severe, and hence giving lower strengths, this is clearly not universally so.

An important question is what are the spatial and size distributions of machining flaws. At present, only partial indications of these distributions exist. Thus, for example, fracture surfaces have been examined for machining flaws other than the one from which failure initiated. Such examinations are most definitive in the smooth, fracture mirror, area since machining flaws, especiallly smaller ones, will generally be partly or totally obscured in the hackle and crack branching regions of fracture [12]. Thus, more area is seen on weaker specimens which could bias the results. However, such observations do give a preliminary idea of flaw distributions, e.g. other machining flaws 10-50% the size of the one causing failure have been reported within $\sim$ 100-300 μm along ground surfaces of fine grain MgF_2 and As_2S_3 glass [4]. Similarly note other machining flaws near the fracture origins of specimens in figures 7-9. Finally, one other preliminary indication of flaw distributions are slow crack growth observations in hot pressed Si_3N_4 (HPSN). At elevated temperatures, flaws begin to open up on tensile surfaces of HPSN due to local deformation, presumably predominantely by grain bound-
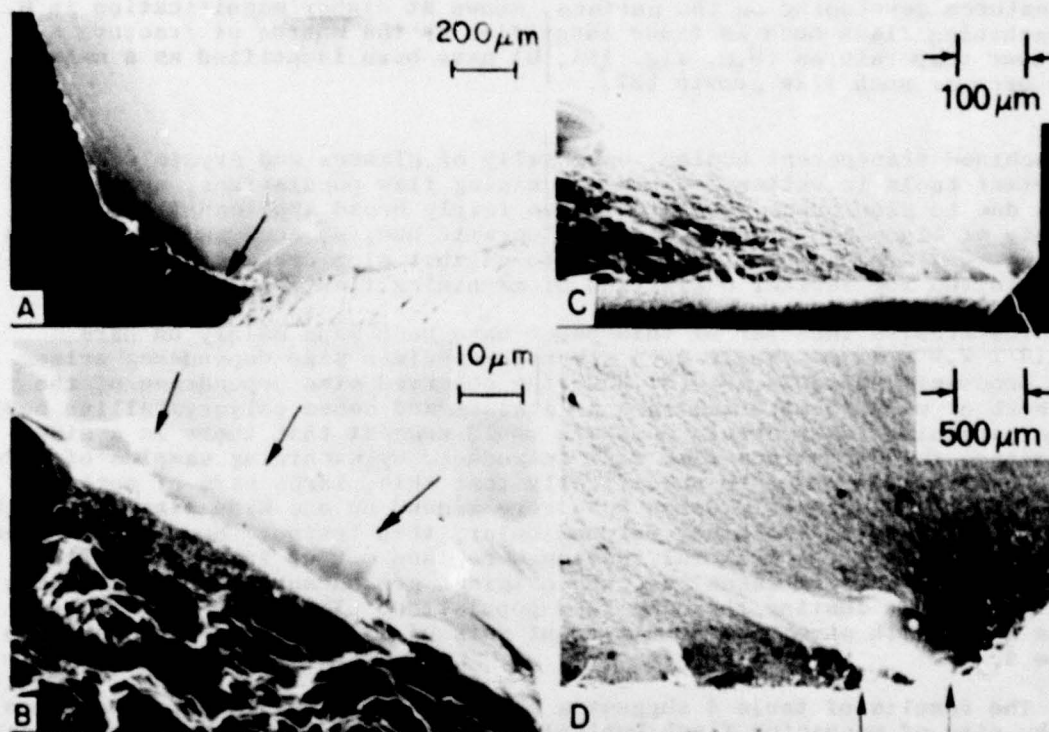

Figure 15. Examples of specific failure causing flaws at specimen edges. A and B are photos of the area of origin and specific fracture origin (arrows) in a single crystal of CaO stabilized ZrO_2, failure stress 105 MPa (15,300 psi). C and D are fracture photos of the area of origin and actual origin (arrows) of a failure causing flaw at the edge of a hot pressed MgF_2.

21

ary sliding. These opening cracks appear to often originate from larger machining flaws (some cases of this have been verified [21]). Therefore, the distribution of these opening cracks gives some idea of the surface density of flaws, e.g. figure 16. While controlled, e.g. side, lighting, or etching
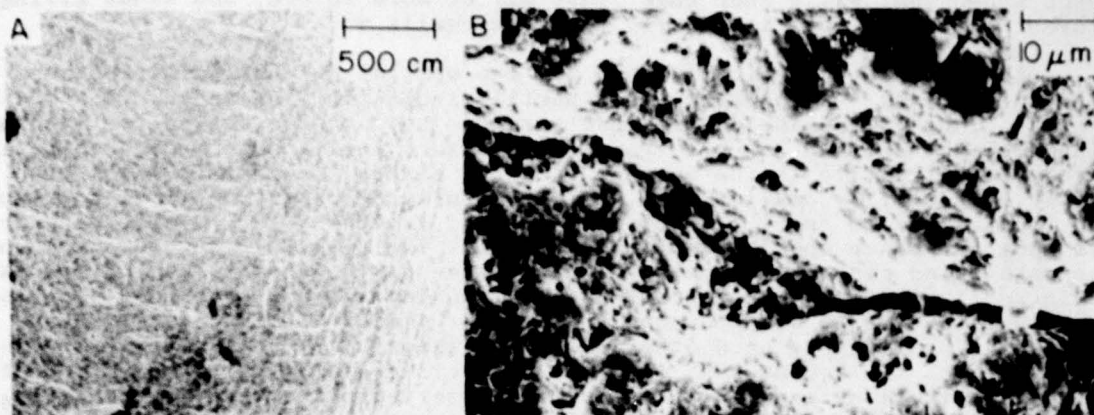

Figure 16.   Example of slow crack growth opening of machining flaws.   A and B show hot pressed Si_3N_4 (HS-130) tensile creep rupture tested at ~ 87 MPa (12,500 psi) at 1300°C (failure strain ~ 13.8 x 10^{-3}).   Note the ~ linear features developing on the surface, shown at higher magnification in B. Machining flaws such as those identified as the source of fracture at lower temperatures (e.g. fig. 18A, B) have been identified as a major source of such flaw growth [21].

of machined transparent bodies, especially of glasses and crystals can be important tools in better defining machining flaw populations, opening of flaws due to slow crack growth may have fairly broad applicability. Thus, a variety of Al_2O_3 and other commercial ceramic bodies, such as crystallized glasses [33] are known, or expected, to exhibit slow crack growth that could be exploited for further definition of machining flaw populations.

The studies thus far of this paper have been made mainly on bars ~ 1.3 x 2.6 x 13 mm. While much strength-specimen size dependence arises from processing defects [5,6,34,35], the observed size dependence of the strength of ceramic material such as glasses and dense polycrystalline bodies where machining flaws should dominate would suggest that there is a size dependence to the maximum flaw size introduced by machining samples of different sizes.   In order to specifically test this, large bars of optical grade, fully dense, hot pressed MgF_2 were ground on one side parallel to the tensile axis and on the other perpendicular, then tested. Sections of these large MgF_2 bars after flexural testing were then cut up into smaller test bars whose tensile surfaces were the original ground surfaces of the large bars so we were testing the same flaw population.   The results of these tests along with some data on different sets of B_4C specimens are shown in table 4.

The results of table 4 suggest a possible effect of the specimen size on the size of machining flaws controlling strengths, but several complications occur. First, since the same head travel rate was used, the strain rates were lower for larger bars allowing more slow crack growth to occur; thus strain rate is being held constant in other tests of MgF_2 and SiO_2 based glasses now underway. Second, processing defects (and possibly variations in B_4C) play a larger role in the failure of larger bars, limiting the machining results. Third, both MgF_2 and B_4C have internal stresses due to their non-cubic crystal structures which limit the increases in strength with decreasing flaw size [36]. Thus, while the strength results do not

22

strongly show a size effect, the flaw observations more strongly indicate
such an effect. In order to minimize these complications, additional tests
are now under way on SiO₂ based glasses. However, initial results have been
complicated by different types of flaws being common sources of failure in
many of the large bars. These flaws represent either handling damage (which
could be much more severe in larger, i.e. more massive, bars), or a new, much
more limited population of machining induced flaws, e.g. from such possible
effects such as damage from unusually large swarf particles trapped between
the specimen and grinding wheel.* Other indications that a size effect for
machining flaws may exist, but may generally be limited, are shown by frac-
ture origins of components or prototypes, e.g. figures 17, 18, and refer-
ences 5,16,18, and 19. These suggest somewhat deeper flaws than in test bars,
but specimen shape may also be a factor. Thus, the data of Bansal and Duck-
worth on Pyroceram 9606 [34] reporting no size effect of machining is not
necessarily at conflict with the preliminary studies. Either their material
or machining may have produced limited changes in machining flaw sizes not
discernable in the limited number of observations made. (Again, possible
effects of internal stresses could limit strength differences between differ-
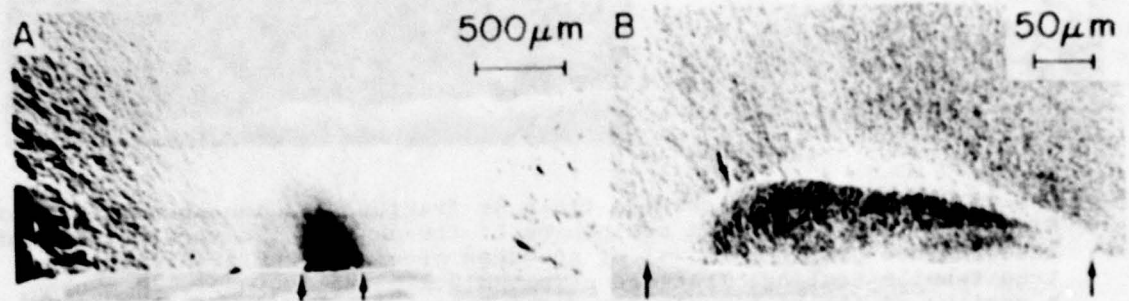ent size bars with different size flaws.)

Figure 17. Photos of the area of fracture origin and actual origin (arrows)
of a polished, IR dome, MgF₂ failed in a simulated aero-thermal heating
test. The failure stress of ~ 69 MPa (10,000 psi) estimated from the ob-
served flaw size and the measured fracture energy and Youngs modulus is
in excellent agreement with the failure stress predicted from thermal
analysis. Note the similarity in size and shape of this flaw in a pol-
ished component to that shown earlier in figure 11 in a polished MgF₂ disk.

---

*Another possible source of different flaws are those formed at the edge of
the grinding wheel on larger bars that are wider than the wheel in contrast
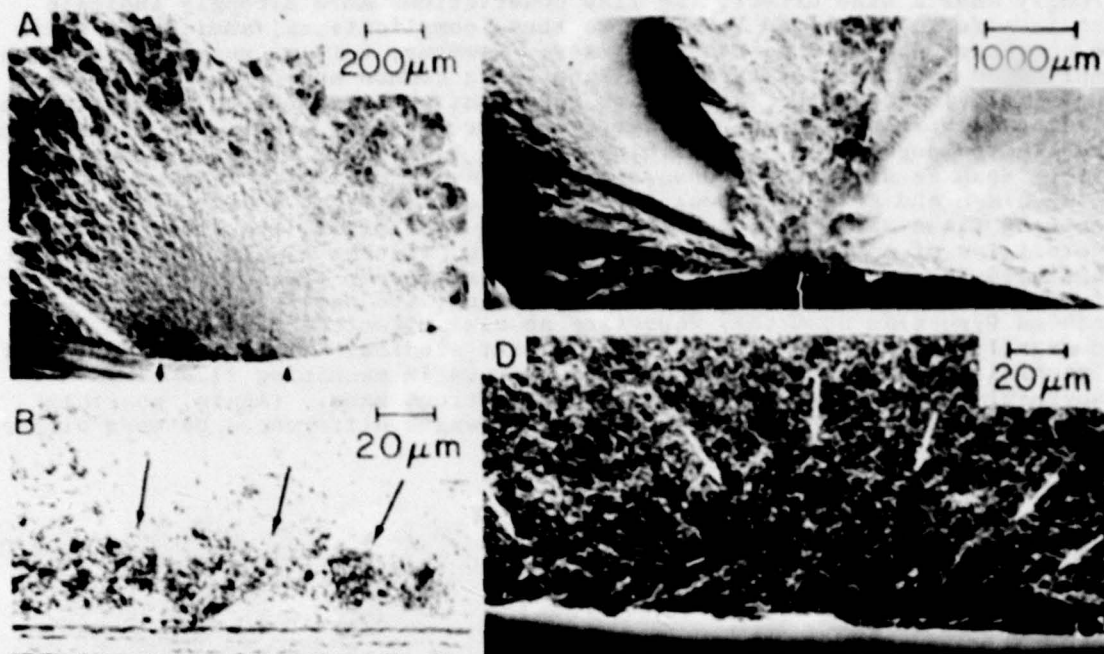to small bars which are narrower than the wheel.

23

Figure 18. Examples of machining flaws at fracture origins in hot pressed
Si₃N₄ (NC-132). A and B are photos of the area of fracture origin and
the fracture origin (arrows) of specimen ground circumferentially for
true tensile testing; fracture stress 312 MPa (45,300 psi). B shows
a portion of the highly elongated flaw which is about average in defini-
tion for such flaws in Si₃N₄. Other clearer examples of these types of
flaws can be found in references 20 and 21. C and D show the fracture
origin area and fracture origin (arrows) in a simple prototype Si₃N₄
turbine blade spun tested to failure at room temperature. The specimen
(courtesy of Mr. Dave Richerson, Garrett Airesearch) failed in the attach-
ment area where stresses are highest and machining is perpendicular to
the blade (tensile) axis; failure stress was ~ 483 MPa (70,000 psi). Note
the Richerson and Yonushonis [37] have shown similar, clearer examples of
such fracture origins in failed turbine blades.

5. Summary and Conclusions

Fractography has been used to identify machining flaws controlling the
strengths of a variety of ceramic bodies. This shows that sawing, grinding,
sanding, and polishing all introduce predominately two populations of flaws
extending in from the surface. One set, those giving the lowest strengths
are formed essentially parallel with the machining grooves formed by the grit
particles and are generally fairly elongated. The other set of flaws, those
typically giving higher strengths, are typically formed perpendicular to the
machining grooves and are generally less elongated, often approaching a semi-
circular periphery. The differences in size and shape in these two sets of
flaws combined with their orientation relative to the direction of machining
are the predominate cause of the anisotropy of strength as a function of the
stressing direction relative to the direction of machining.

24

Variations in the depth, shape, and orientation of the above sets of flaws have been observed, as well as effects of composition and microstructure. While some variations in flaw orientation appear to be sporatic in larger grain bodies where flaws are similar to or less than the grain in size, and especially in single crystals, the orientation of preferred cleavage planes can be an important factor. The set of generally elongated flaws that typically form parallel with the machining grooves vary from a continuous flaw to a series of partially overlapping flaws. Flaws forming generally perpendicular to machining grooves often have a fan and curved character, e.g. like half a clam shell. No obvious effect of body composition is seen on the size, i.e. depth, of either set of flaw introduced, and decreasing grain size has at best a limited effect on reducing the size of the strength controlling flaws introduced. Thus, the typical variety of machining processes commonly introduce flaws in the range of 20-50 μm depth for both sets of flaws in glasses, single crystals, and typical grain size dense polycrystals in most laboratory size test bars. Limited evidence, as well as the statistical nature of machining flaws, both suggest that the size of machining flaws controlling strength increases some with specimen or component size. However, increasing competition from other flaws, e.g. processing flaws or flaws introduced by handling processes limit such machining flaw size-specimen size evaluation.

Note added in Proof

Two factors, slow crack growth and residual stresses, not addressed in the text should be briefly considered. While slow crack growth might increase flaw sizes by 50-100% in the extreme, this would not change the strength anisotropy unless the growth was significantly different for the two populations of flaws. The generally good agreement between measured strength anisotropy and that calculated from observed flaws argues against significant differences in flaw growth. Further, fracture energies calculated from observed flaw sizes generally agree with measured values [9,20-23,36] unless altered by other factors such as thermal expansion anisotropy [36], indicating flaw growth in most of these materials is limited, e.g. < 50%. If residual stresses in the surface from machining were compressive in nature, they would compensate, at least in part, for slow crack growth. On the other hand, if residual stresses are tensile, e.g. as indicated in recent indentation tests (private communication with Dr. Brian Lawn) then their effects would be additive to those of slow crack growth. Again, the above results indicate that any additive effects are limited. Thus, while further study of slow crack growth and residual stress are important to refine our understanding of machining flaw-mechanical property relations, they do not appear to require major changes in the results and conclusions of this study.

TABLE 4

SPECIMEN SIZE-STRENGTH[1] AND FLAW SIZE EFFECTS IN GROUND BARS

Ground ⊥[2]				Ground ∥[2]			
Strength		Flaw[3]		Strength		Flaw[3]	
ksi	MPa	a(μm)	b/a	ksi	MPa	a(μm)	b/a

MgF$_2$ (KODAK, HOT PRESSED, ~ 0 POROSITY, GRAIN SIZE ~ 0.5 μm)

Span 4 cm, cross section 1 x 1.8 cm:

11±2	76±14	75±20	4±2	12±2	80±14	-	-
(4)		(4)		(3)			

Span 1.27 cm, cross section 0.51 x 0.25 cm:

12±1	80±7	42±3	~ 4	16±3	110±20	57±11	0.8±0.3
(4)		(3)		(9)		(3)	

B$_4$C (NORTON, HOT PRESSED, < 1% POROSITY, GRAIN SIZE ~ 10 μm)

Span 2.54 cm, cross section 1.27 x 0.60 cm:

35±4	240±27	100±80	1.1±0.2	44±6	304±40	60±40	1±0.5
(4)		(3)		(4)		(3)	

Span 1.27 cm, cross section 0.62 x 0.24 cm:

34±12	235±80	18±3	3±1	49±6	338±40		
(7)		(3)		(7)			

B$_4$C (FIBER MATERIALS, HOT PRESSED, < 1% POROSITY, GRAIN SIZE ~ 2 μm)

Span 1.9 cm, cross section 0.51 x 0.25 cm:

19±2	130±14	29±11	4±1	47±12	325±80	13±8	2±1.8
(5)		(4)		(5)		(3)	

---

[1] Strengths measured at 23°C in 3 point flexure with a head travel rate of ~ 1.27 mm/min.

[2] ⊥ and ∥ refer respectively to the direction of grinding relative to the bars' tensile axis. Lower numbers in parentheses give the number of values. The fewer number of values for flaw parameters than strengths reflect failure from processing defects or specimen edges.

[3] a = flaw depth, b = flaw length along surface.

References

[1] Rice, R. W., Panel Discussion, in The Science of Ceramic Machining and Surface Finishing, NBS Special Pub. 348, 407-408, S. J. Schneider and R. W. Rice, eds. (Govt. Printing Office, Wash., D.C. 20402, 1972).

[2] Mecholsky, J. J., Freiman, S. W., and Rice, R. W., Effect of Grinding on Flaw Geometry and Fracture of Glass, J. Am. Ceram. Soc. [60] 3-4 (1977).

[3] Mecholsky, J. J., Freiman, S. W., and Rice, R. W., Effect of Surface Finish on the Strength and Fracture of Glass, Proc. of the XIth Int. Congress on Glass, Prague, Czechoslovakia (1977).

[4] Rice, R. W., Machining of Ceramics, in Ceramics for High-Performance Applications, 287-243, Proc. of 2nd Army Materials Technology Conf., Hyannis, Mass (1973).

[5] Rice, R. W., Mecholsky, J. J., Freiman, S. W. and Morey, S. M., to be published in Proc. in Quantative NDE Conf. , Cornell Univ., Air Force Report #AFML-TR-77 (1977).

[6] Rice, R. W., Processing Induced Sources of Mechanical Failure in Ceramics, in Proc. of Conf. on the Processing of Crystalline Materials, H. Palmour III, R. F. Davis, and T. M. Hare, eds., 303-319 (Plenum Press, 1978).

[7] Rice, R. W., Microstructure Dependence of Mechanical Behavior of Ceramics, in Treatise on Materials Science and Technology, Vol. 11, Properties and Microstructure, 199-381 (Academic Press, N.Y., 1977).

[8] Freiman, S. W., Mecholksy, J. J., Rice, R. W. and Wurst, J. C., Influence of Microstructure on Crack Propagation in ZnSe, J. Am. Ceram. Soc. [58] 9-10, 406-409 (1975).

[9] Rice, R. W., Mecholsky, J. J. and Becher, P. F., The Effect of Grinding Direction on Flaw Character and Strength of Single Crystal and Polycrystalline Ceramics, to be submitted to J. Am. Ceram. Soc.

[10] Rice, R. W., Machining, Surface Work Hardening, and Strength of MgO, J. Am. Ceram. Soc. [56] 10, 536-541 (1973).

[11] Rice, R. W., The Effect of Grinding Direction on the Strength of Ceramics, in The Science of Ceramic Machining and Surface Finishing, NBS Special Pub. 348, 365-376, S. J. Schneider and R. W. Rice, eds., (Govt. Printing Office, Wash., D. C. 20402, 1972).

[12] Rice, R. W., Fracture Topography of Ceramics, in Surfaces and Interfaces of Glass and Ceramics, 439-472, V. D. Frechett, W. C. LaCourse, and V. L. Burdick, eds. (Plenum Press, N. Y. 1974).

[13] Kirchner, H. P., Gruver, R. M. and Walker, R. E. Strength Effects Resulting from Simple Surface Treatments, in The Science of Ceramic Machining and Surface Finishing, NBS Spec. Pub. 348, 353-363, S. J. Schneider and R. W. Rice, eds. (Govt. Printing Office, Wash., D. C. 20402, 1972).

[14] Richerson, D. W., Schuldies, J. J., Yonushonis, T. M. and Johansen, K. M., ARPA/Navey Ceramic Engine Materials and Process Development Summary, in Proc. of 5th Army Materials Technology Conf. on Ceramics for High Performance Applications-II, J. J. Burke, E. N. Lenoe and R. N. Katz, eds. (Brook Hill Pub. Co., Mass. 1978).

[15] Gielisse, P. J., Kim, T. J. and Choudry, A., Dynamic and Thermal Aspects of Ceramic Processing, Naval Air Systems Command Contract Report, 15 Nov 1970-15 Nov 1971, Univ. of Rhode Island, Ingston (Dec. 1971, AD 740 833).

[16] Tressler, R. E., Langensiepen, R. A. and Bradt, R. C., Surface-Finish Effects on Strength-vs-Grain Size Relations in Polycrystalline Al_2O_3, J. Am. Ceram. Soc. [57] 5, 226-227 (1974).

[17] Bradt, R. C., Dulberg, J. L. and Tressler, R. E., Surface Finish Effects and the Strength-Grain Size Relationship in MgO, Acta Metallurgic [24] 529-534 (Pergamon Press, Great Britain, 1976).

[18] Cranmer, D. C., Tressler, R. E. and Bradt, R. C., Surface Finish Effects and the Strength-Grain Size Relation in SiC, J. Am. Ceram. Soc. [60] 5, 230-237.

[19] Bradt, R. C. and Tressler, R. E., Microstructure/Surface Finish Control of the Strength of Polycrystalline Ceramics, Proc. of 6th Int. Mat. Symposium on Ceramic Microstructures, 76, R. M. Fulrath and J. A. Pask, eds., 785-795 (Westview Press, Boulder, Colorado, 1976).

[20] Rice, R. W., Freiman, S. W., Mecholsky, J. J., Ruh, R. and Harada, Y., Fractography of Si_3N_4 and SiC, in _Ceramics for High Performance Applications-II_, Proc. of 5th Army Materials Technology Conf., J. J. Burke E.N.Lenoe and R.N.Katz, eds. (Brook Hill Publishing Co., Chestnut Hill, MA, 1978).

[21] Rice, R. W., Freiman, S. W. and Mecholsky, J. J., Fracture Sources in Si_3N_4 and SiC, Proc. of 1977 DARPA/NAVSEA Ceramic Gas Turbine Demonstration Engine Program Review, 665-688, J. W. Fairbanks and R. W. Rice, eds. Maine Maritime Academy, Castine, Maine, 1-4 Aug 1977 (MCIC 78-36).

[22] Rice, R. W., Machining Flaws and the Strength-Grain Size of Ceramics, this conference.

[23] McDonough, W. J., Flinn, D. R., Stern, K. H. and Rice, R. W., Hot Pressing and Physical Properties of Na Beta Alumina, J. Mat. Sci., 13, 2403-2412 (1978).

[24] Richerson, D. and Yonushonis, T., in _Ceramic Gas Turbine Engine Demonstration Program_, Interim Report #4, 4-8 to 4-10, Airesearch Report #76-212188(4), Contract #N00024-76-C-5352 (1977).

[25] Brüche, E. and Poppa, H., Zur Kenntnis der Glasoberfläche, Electron Microscopy, 336-338, F. S. Sjostrand and J. Rhodin, eds. (Academic Press, New York, 1956).

[26] Imanaka, O., Lapping Mechanics of Glass-Especially on Roughness of Lapped Surface, Annals of the C.I.R.P., Vol. XIII, 227-233 (Pergamon Press, 1966).

[27] Allgeyer, G. H. and Colwell, L. V., Aspects of Machining Glass-Ceramic Materials, in _The Science of Ceramic Machining and Surface Finishing_, NBS Special Pub. 348, 53-57, S. J. Schneider and R. W. Rice, eds (Govt. Printing Co., Wash., D.C. 20402, 1972).

[28] Brian, L. and Wilshaw, R., Review Indentation Fracture: Principles and Applications, J. Mat. Sci. [10], 1049-1081 (1975).

[29] Evans, A. G., Abrasive Wear Damage in Brittle Materials, this conference.

[30] Doremus, R. H., Johnson, W. A., Depths of Fracture-Initiating Flaws and Initial Stages of Crack Propagation in Glass, J. Mat. Sci., 13, 855-858 (1978).

[31] Mecholsky, J. J. Fractographis Analysis of Delayed Failure in MgF_2, submitted to J. Am. Ceram. Soc.

[32] Dutta, S., Rice, R., Graham, H. and Mendiratta, M., Characterization and Properties of Controlled Nucleation Thermo Chemical (CNTD) Deposited Silicon Carbide, to be published.

[33] Govila, R. K., Kinsman, K. R. and Beardmore, P., Fracture Phenomenology of a Lithium-Aluminum-Silicate Glass-Ceramics, J. Mat. Sci., 13, 2081-2091 (1978).

[34] Bansal, G. K., Duckworth, W. H. and Niesz, D. E., Strength-Size Relationships in Ceramic Materials: Investigation of a Commercial Glass-Ceramic, J. Am. Ceram. Soc. [55] 3, 289-308 (1976).

[35] Bansal, G. K., Duckworth, W. H. and Niesz, D.E., Strength Size Relationships in Ceramic Materials: Investigation of an Alumina Ceramics, J. Am. Ceram. Soc. [59], 11-12, 472-478 (1976).

[36] Rice, R. W., Pohanka, R. C. and McDonough, W. J., The Effect of Stresses from Thermal Expansion Anisotropy, Phase Transformations and Second Phases on the Strength of Ceramics, submitted for publication.

[37] Richerson, D. and Yonushonis, T., in Ceramic Gas Turbine Engine Demonstration Program, Interim Report #5 , 3-9 to 3-11, Airesearch Report #76-212188(5), Contract #N00024-76-C-5352 (1977).